A Universal Framework for the Effect of Operating Parameters on Piezoionic Voltage Generation

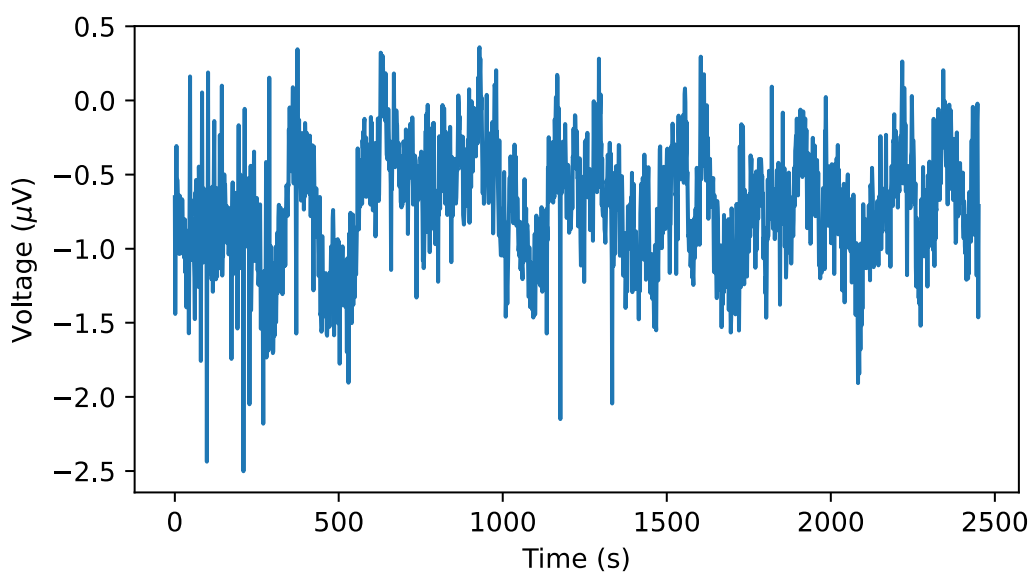Jiangang Xu[ab], Qiang Li[ab], and Derek Ho[ab]*

[a]Department of Materials Science and Engineering, City University of Hong Kong, Kowloon 999077, Hong Kong, China
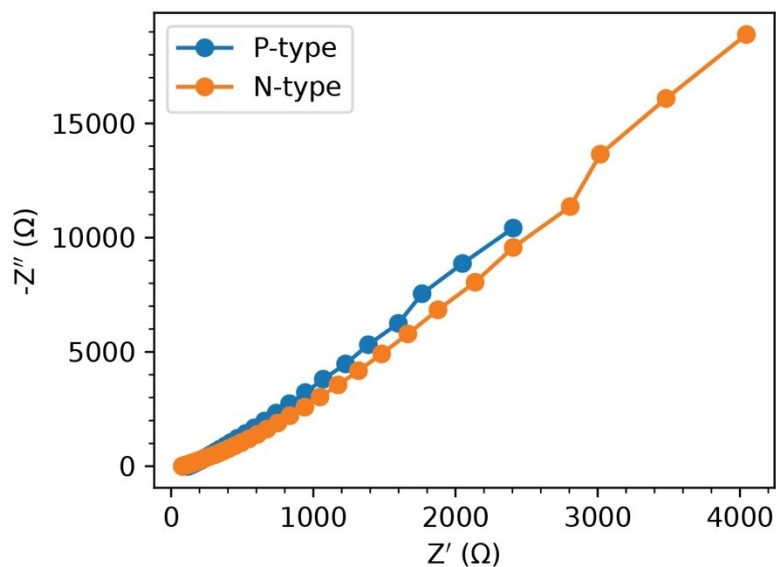[b]Hong Kong Centre for Cerebro-cardiovascular Health Engineering, N.T. 999077, Hong Kong, China
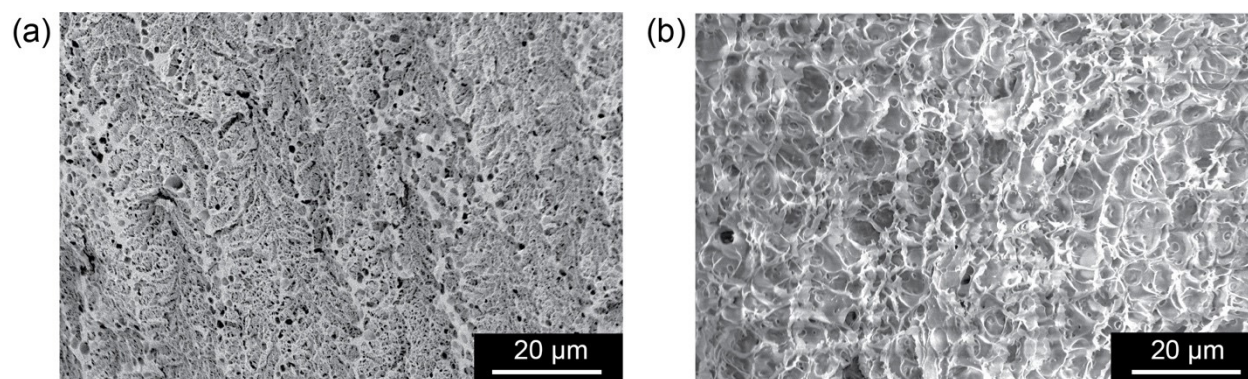Email: derekho@cityu.edu.hk

Supplementary Information

Figure S1. Open circuit voltage (OCV) of a piezoionic device as a function of time.

Figure S2. Nyquist plot of EIS spectra for the P-type and N-type piezoionic hydrogels.

Figure S3. Scanning electron microscopy (SEM) images of piezoionic hydrogels: (a) P-type and (b) N-type. Both samples have a porous structure.

The P-type and N-type piezoionic hydrogels are characterized by SEM. The samples for SEM were prepared by first freezing the hydrogels through immersing them in liquid nitrogen then dried in a freeze dryer. A thin Au layer was sputtered on the samples to increase its electrical conductivity. From the SEM images, porous structures for both hydrogels are evident. Such porous structure confirms our use of poroelasticity theory in the finite element simulation is legitimate.
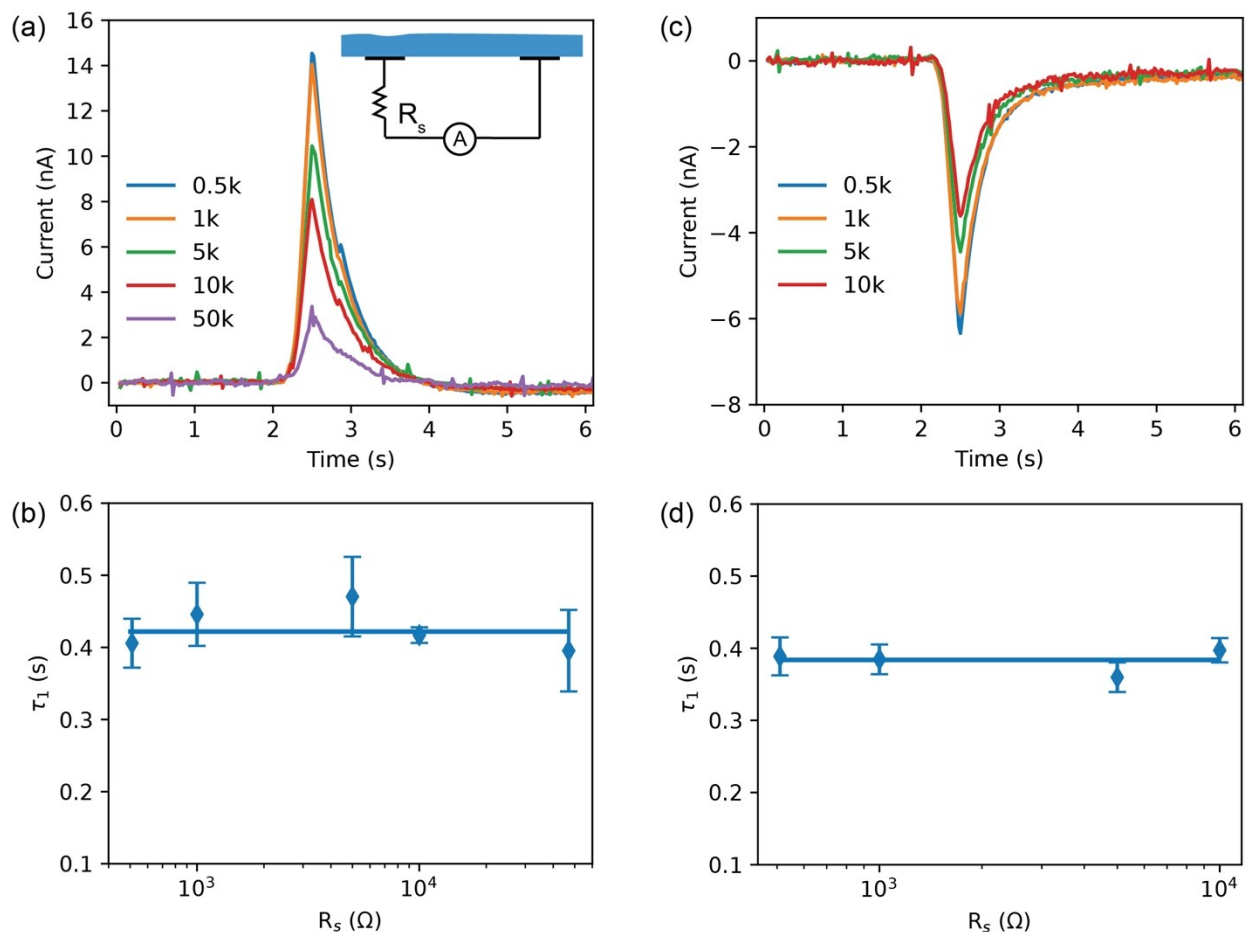
Figure S4. Experiments results for eliminating inadvertent electrical double layer (EDL) charge contribution to the measured signal. (a) Zoom-in view of the measured current during indentation. Evidently, transient peaks are observed. Insert: A resistor R_s is connected in series in the circuit during current measurement for a P-type piezoionic hydrogel. (b) The characteristic time constant of the peak as a function of R_s, showing the time constant is insensitive to the R_s. (e) and (f) show that the time constant is also insensitive to R_s in an N-type piezoionic device.

As the piezoionic device operates in a complex electro-mechano-chemical environment, there could be five major interfering sources that might give spurious voltage contribution to the output OCV, namely, electrochemical reaction, stress induced electrode potential change,[1, 2] Donnan potential due to hydrogel compression under indentation,[3] inadvertent charging of the electrical double layer (EDL) formed at the interface between the electrode and the hydrogel, and voltage generation due to triboelectric effect.[4-6] As we use carbon nanotubes, which are inert, to form the electrodes, electrochemical reaction is not expected in our device. In addition, as long as the hydrogel is maintained in the indented condition, voltage generation from the stress induced electrode potential or the Donnan potential persists, i.e., static response, which is different from the transient behavior in the streaming potential scenario. Therefore, signals from the former three interfering contributions, i.e., electrochemical reaction, stress induced electrode potential change, and Donnan potential, can be eliminated.

Characteristic time constant of the transient peaks in current measurements can be used to eliminate the interference due to inadvertent EDL charging. Specifically, by closing the testing circuit with a resistor R_s in series, the generated voltage from the piezoionic effect drives current flow (insert in **Figure S4a**). As the fluid flow induced voltage is transient, the current is also transient (**Figure S4a**). If there is a significant contribution to the output OCV from the inadvertent charging of the EDL, the time constant of the transient peak would increase with R_s according to $\tau \sim RC$, in which $R = R_i + R_s$, where R_i internal resistance. R_i is about ~1.7 kohm from impedance measurement. However, **Figure 4Sb** shows that the time constant remains nearly constant in a P-type piezoionic device despite R_s increases two orders of magnitudes (much greater than R_i). The independence of the time constant on R_s has also been confirmed in an N-type piezoionic device (**Figure S4c** and **S4d**). In other words, inadvertent charging of the EDL can be eliminated by examining the time constant of the transient response peaks.
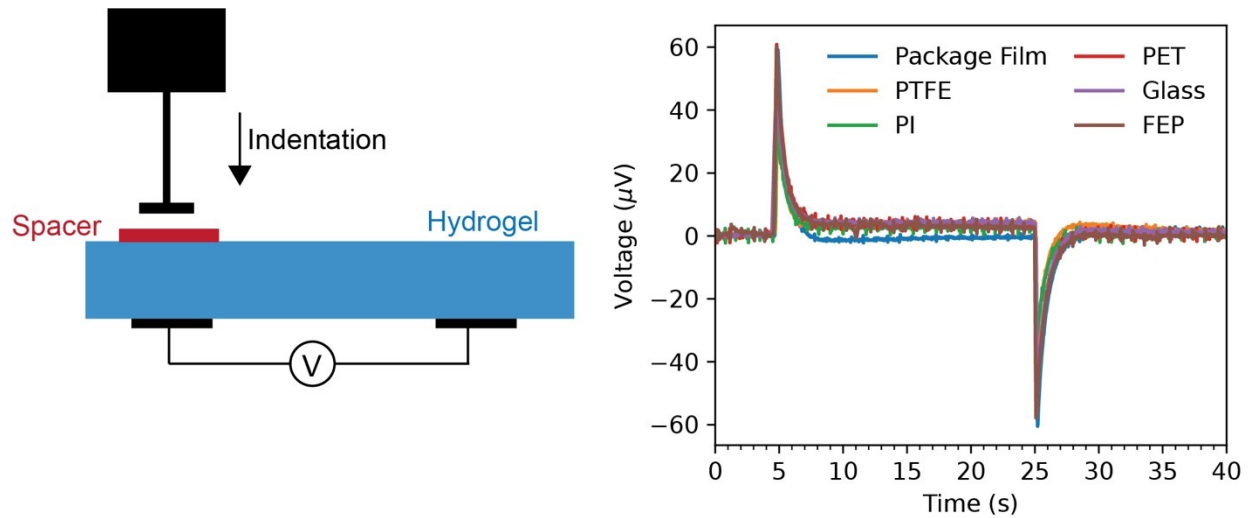

Figure S5. Comparison of the generated voltage of a P-type piezoionic device when a spacer is inserted between the indenter and the hydrogel.

To eliminate any triboelectric contribution to the measured voltage signal, we have applied triboelectric materials[7] including, polytetrafluoroethylene (PTFE), fluorinated ethylene propylene (FEP), polyimide (PI), and non-triboelectric material, e.g., glass, as a spacer, inserted between the indenter and the hydrogel. If there is a significant contribution from triboelectric effect, the measured signals would change drastically. However, as shown in **Figure S5**, the measured voltage across multiple spacers are nearly identical, thus eliminating the possibility of any significant triboelectric contribution to the measured voltage.

Before releasing   At the moment of releasing
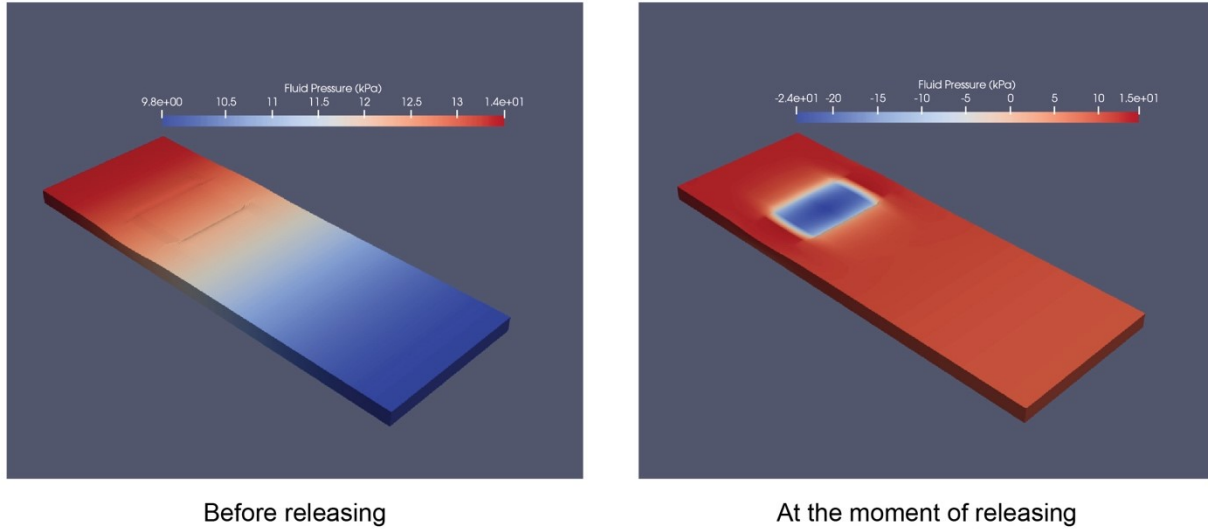
Figure S6. Simulation results showing that at the moment of releasing the stimulus, the fluid pressure at the indented region drops instantly, resulting in a fluid pressure gradient. Such gradient drives fluid flow backwards to the indented region, which leads to the transient recovery peak according to the piezoionic mechanism.
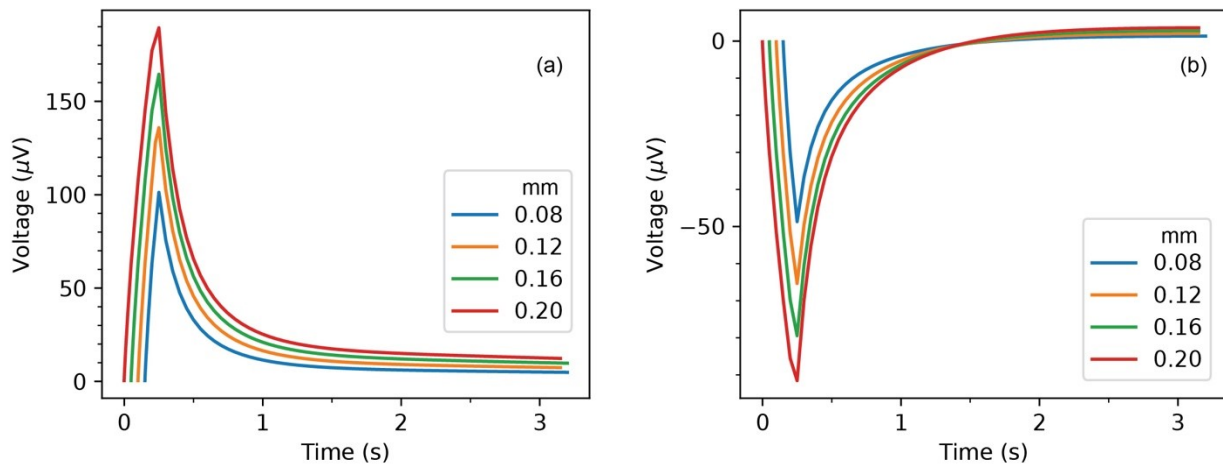
Figure S7. Simulated OCV of (a) a P-type and (b) an N-type piezoionic device when being indented to different depths for a given indentation speed of 50 mm/min.
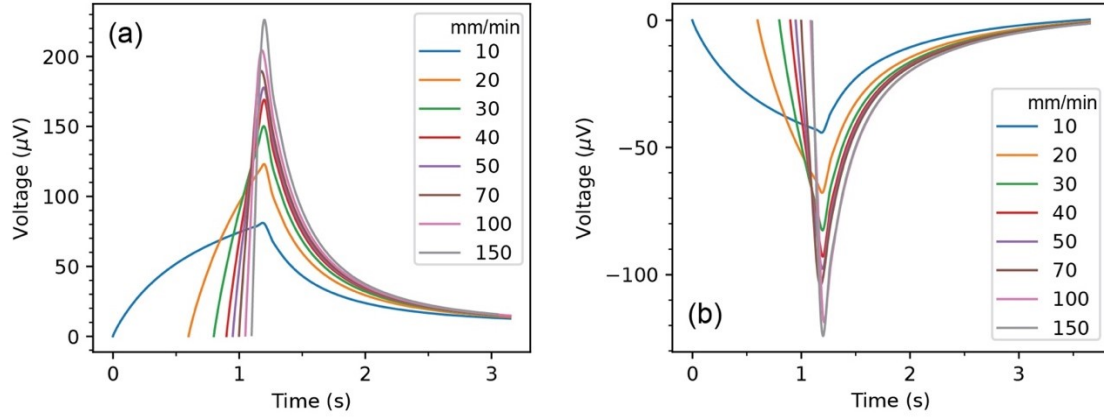
Figure S8. Simulated OCV of a (a) P-type and (b) an N-type piezoionic device when being indented to 0.20mm depth with different indentation speeds.
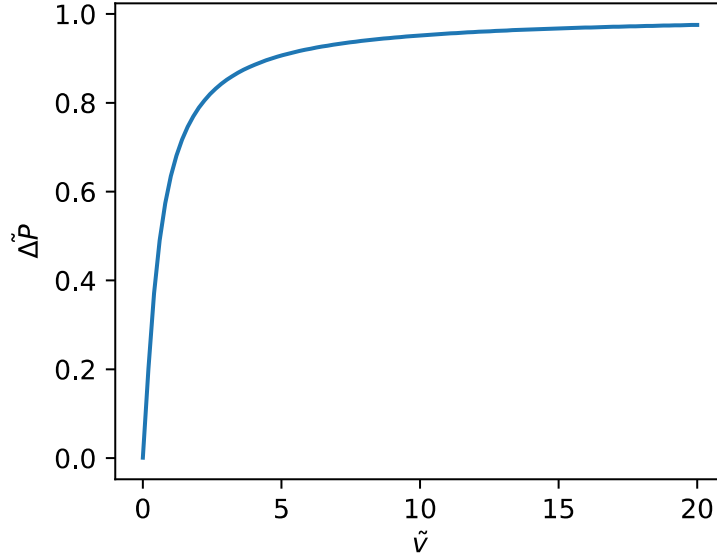
Figure S9. Normalized pressure gradient as a function of the normalized indentation speed. $\Delta P = \tilde{v}(1 - e^{-\frac{1}{\tilde{v}}})$. Evidently, the normalized pressure gradient first increases with the normalized indentation speed then saturates to unity at a higher speed.

Quantitatively, we can use an ordinary differential equation (ODE) to describe the pressure gradient build up process,

$$\frac{d\Delta P}{dt} = -\frac{\Delta P}{\tau} + \alpha v$$

where ΔP is the pressure gradient; $\frac{1}{\tau}$ is the pressure gradient reduction rate by fluid flow, which is relating to the intrinsic properties of the hydrogel and the fluid; v is the indentation speed; α is a coefficient relating the indentation speed to the pressure gradient build up rate. This linear ODE has a solution of the form

$$\Delta P = v\alpha\tau(1 - e^{-\frac{t}{\tau}})$$

As the indentation depth d is fixed, the time for completing the indentation is $t = \frac{d}{v}$. Therefore, we can express the final pressure gradient at the end of indentation as

$$\Delta P = v\alpha\tau(1 - e^{-\frac{d}{v\tau}})$$

To reveal more insights, we can define a characteristic pressure gradient $\Delta P_0 = d\alpha$ and a characteristic fluid flow speed $v_0 = \frac{d}{\tau}$. We then normalize ΔP and v to ΔP_0 and v_0, resulting in $\tilde{\Delta P}$ and $\tilde{v}$, respectively. As a result, we finally have

$$\tilde{\Delta P} = \tilde{v}(1 - e^{-\frac{1}{\tilde{v}}})$$

which first increases with respect to $\tilde{v}$ then saturates to 1 at a larger value of $\tilde{v}$, as shown in **Figure S9**. The competition between the indentation speed and the characteristic fluid flow speed is evident. Specifically, when the indentation speed v is much lower than v_0, equation (4) simplifies to $\tilde{\Delta P} = \tilde{v}$. It is evident that only a very low fluid pressure gradient can be generated, leading to a small final fluid flow speed thus a low output OCV. With an increasing indentation speed v, the pressure gradient and the final fluid flow speed increase, resulting in an increasing OCV. When the indentation speed v is much higher than v_0, equation (4) simplifies to $\tilde{\Delta P} = 1$. As a result, the pressure gradient generated and the final fluid flow speed saturates, thus the piezoionic response is   also   saturated.
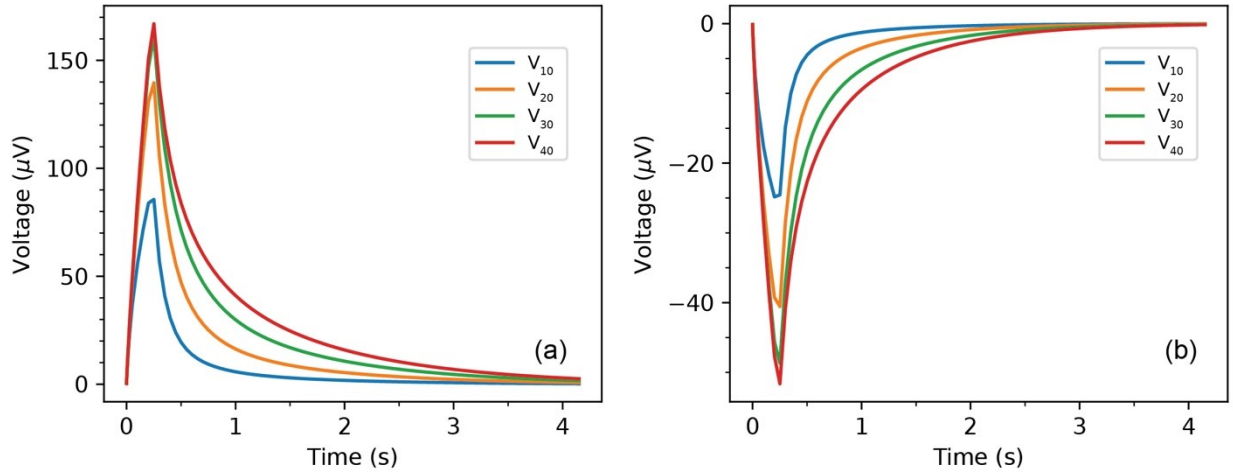
Figure S10. Simulated transient OCV between electrode pairs (E_1, E_0), (E_2, E_0), (E_3, E_0), and (E_4, E_0) in (a) a P-type and (b) an N-type piezoionic device.
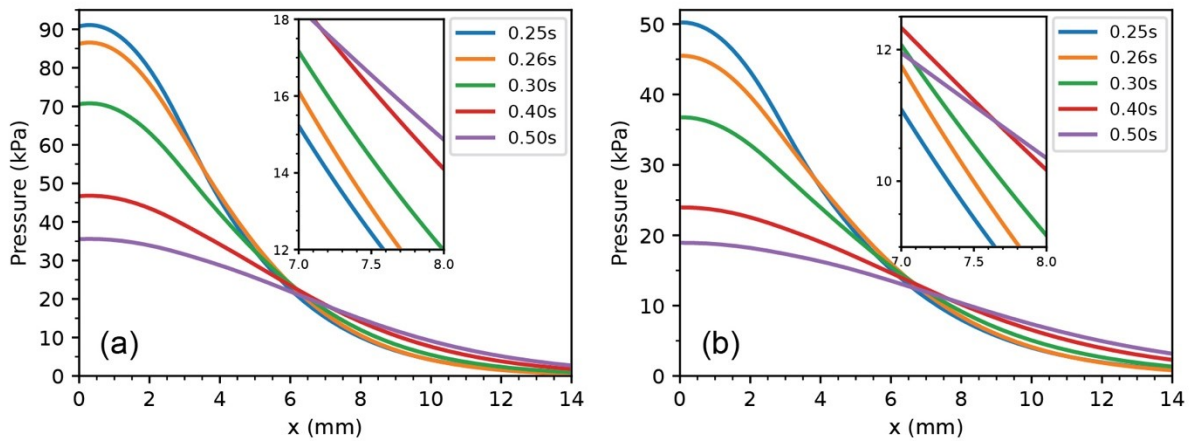
Figure S11. Simulated spatial-temporal distribution of the pressure in (a) a P-type and (b) an N-type piezoionic device. Evidently, the pressure near the indented area ($x \sim 0$ mm) decreases with time, whereas the pressure at distance far away (e.g., $x \sim 7.5$ mm) increases with respect to time, which is indicative of fluid flow.
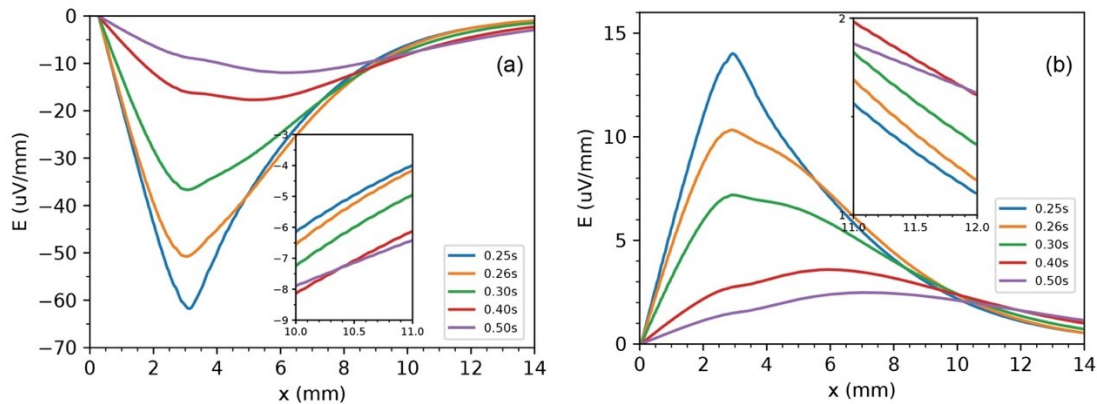
Figure S12. Simulated spatial-temporal distribution of the generated electrical field in (a) a P-type and (b) an N-type piezoionic device. Evidently, the electrical field near the indented area (x ~ 0 mm) decreases with time, whereas the electrical field it at distance far away (e.g., x ~ 10.5 mm) increases with time, which is the result of fluid flow.
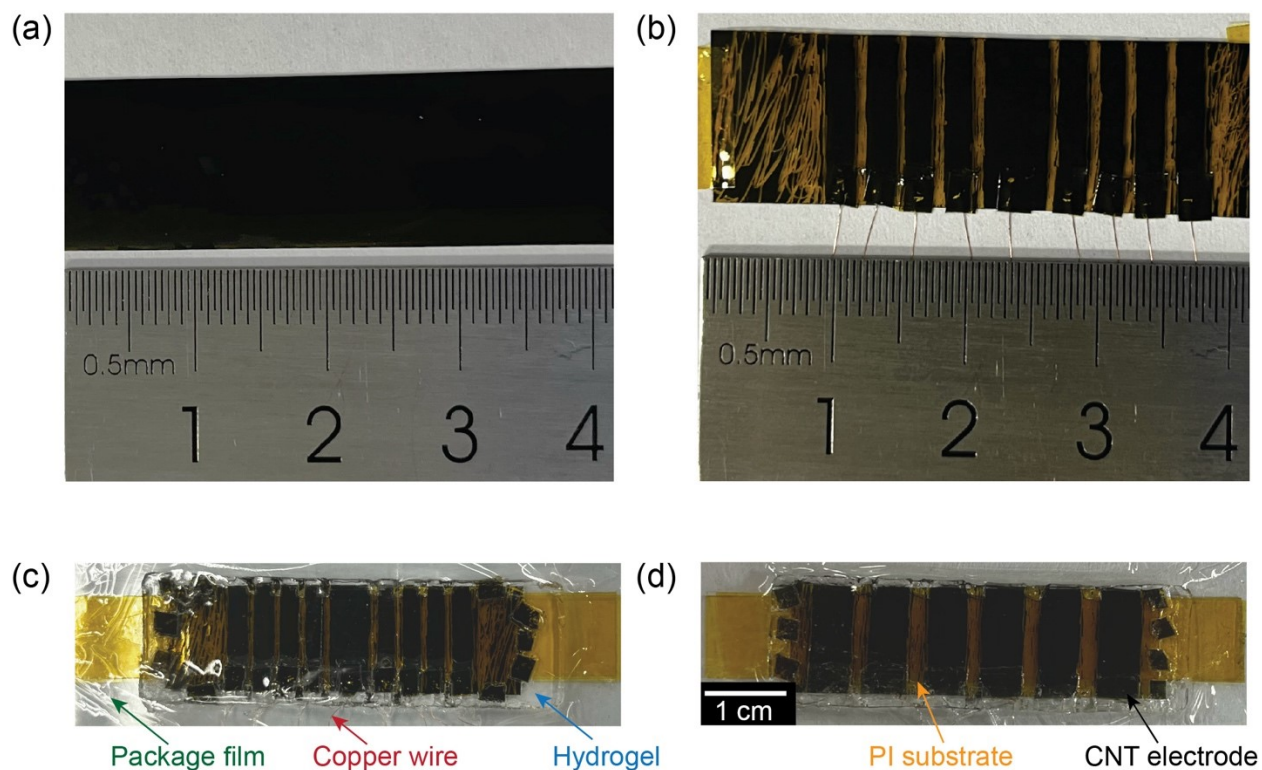

Figure S13. (a) A polyimide (PI) substrate spray coated with a CNT layer. (b) The CNT electrodes were patterned into the desired dimensions by scratching away unwanted regions using a thin pin. The CNT electrodes were then connected with enameled copper wires (the insulation layer here isolates the copper from the hydrogel) using silver paste for subsequent OCV measurements. (c) and (d) Photos of two representative devices used in this study.
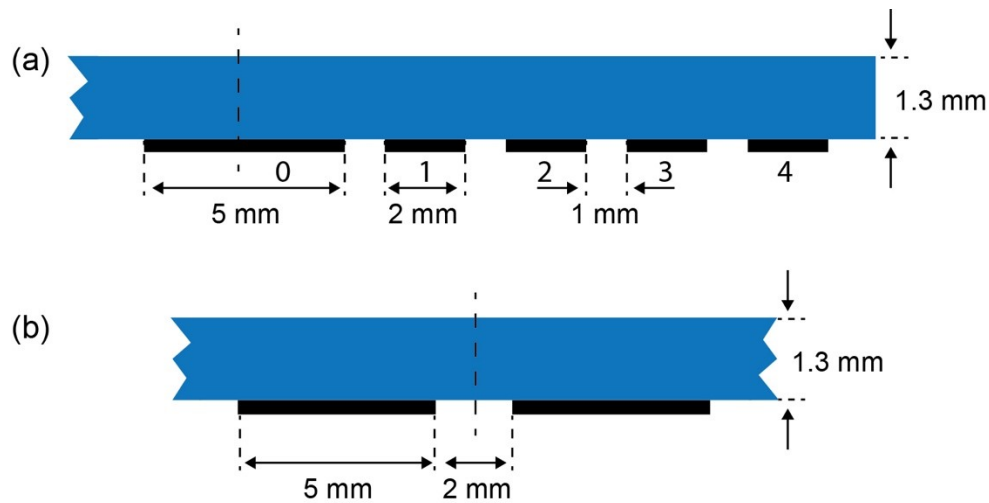
Figure S14 Dimensions of devices used in (a) spatial-temporal measurement and (b) piezoionic dynamics measurement. The hydrogel sample used in experiment is symmetric with respect to the vertical dashed line. The total hdyrogel sample length is 45 mm. Only the part of the sample with electrodes is shown.
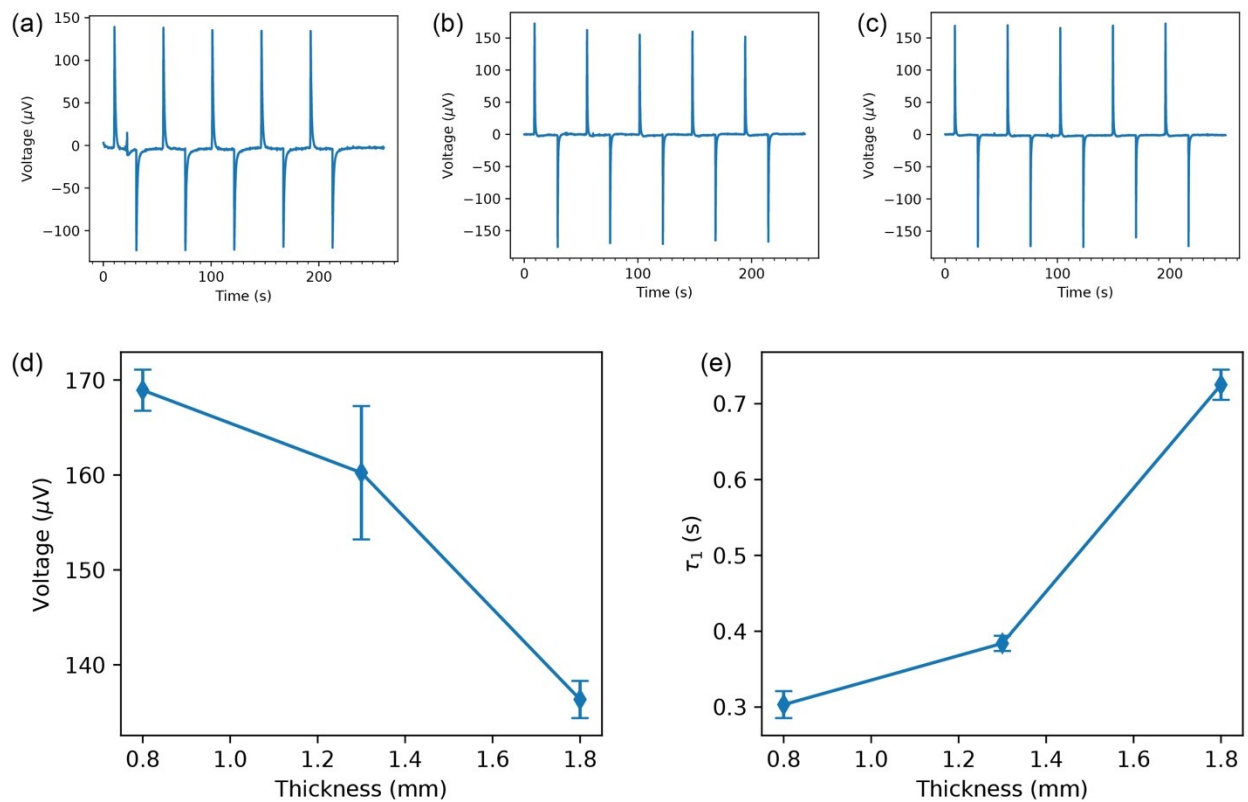
Figure S15. Effect of hydrogel thickness on a P-type piezoionic device. The generated voltage as a function of time in response to periodic indentation for a P-type piezoionic device of thickness of (a) 0.8 mm, (b) 1.3 mm, and (c) 1.8 mm. (d) Voltage amplitude as a function of thickness for a P-type piezoionic device. (e) FWHM of the generated voltage peak as a function of thickness for a P-type piezoionic device.
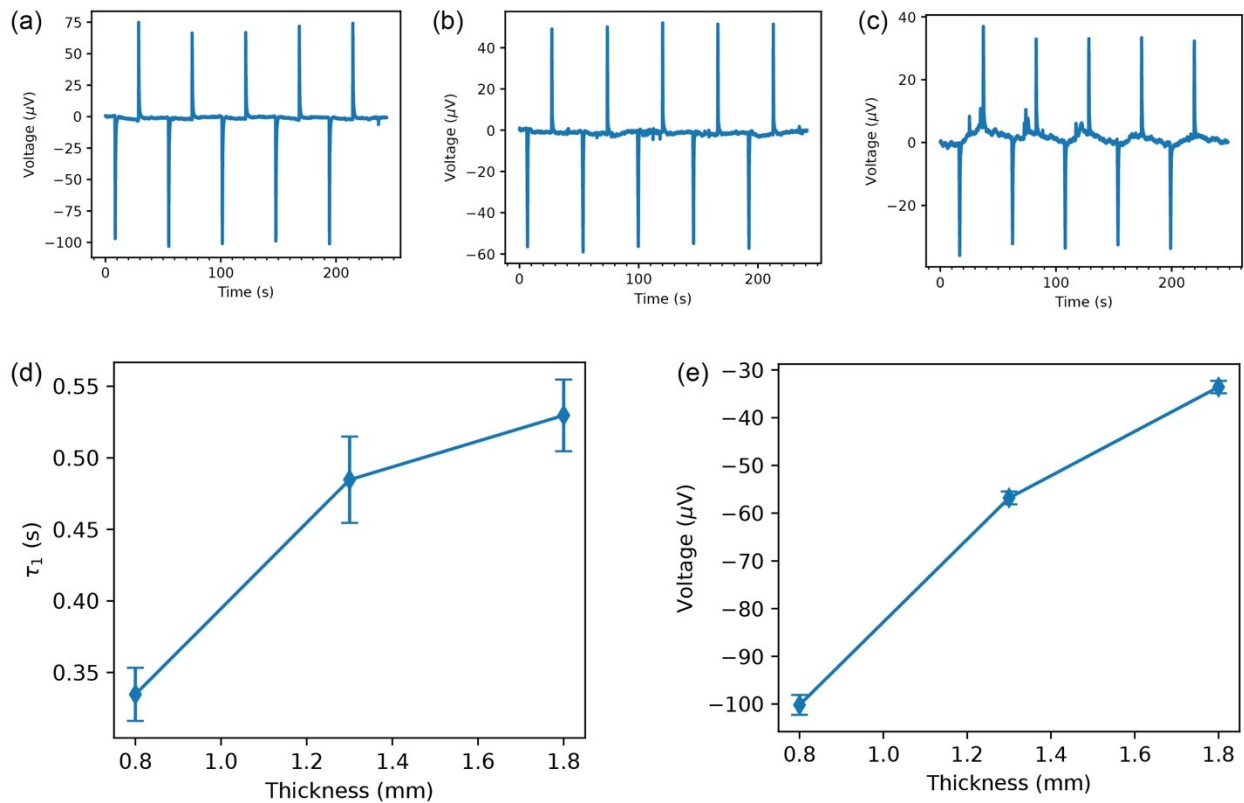
Figure S16. Effect of hydrogel thickness on an N-type piezoionic device. The generated voltage as a function of time in response to periodic indentation for an N-type piezoionic device of thickness (a) 0.8 mm, (b) 1.3 mm, and (c) 1.8 mm. (d) Voltage amplitude as a function of thickness for an N-type piezoionic device. (e) FWHM of the generated voltage peak as a function of thickness for an N-type piezoionic device.

The effect of hydrogel thickness for a P-type and an N-type piezoionic device can be found in **Figure S15** and **S16**, respectively. Evidently, with increasing film thickness, the amplitude of the generated voltage decreases while the FWHM increases with film thickness. This is because a thicker hydrogel results in a lower pressure gradient, thus a slower fluid flow, which leads to a lower generated voltage and wider voltage peak. This generalization is consistent with previously reported prototypes. [4]
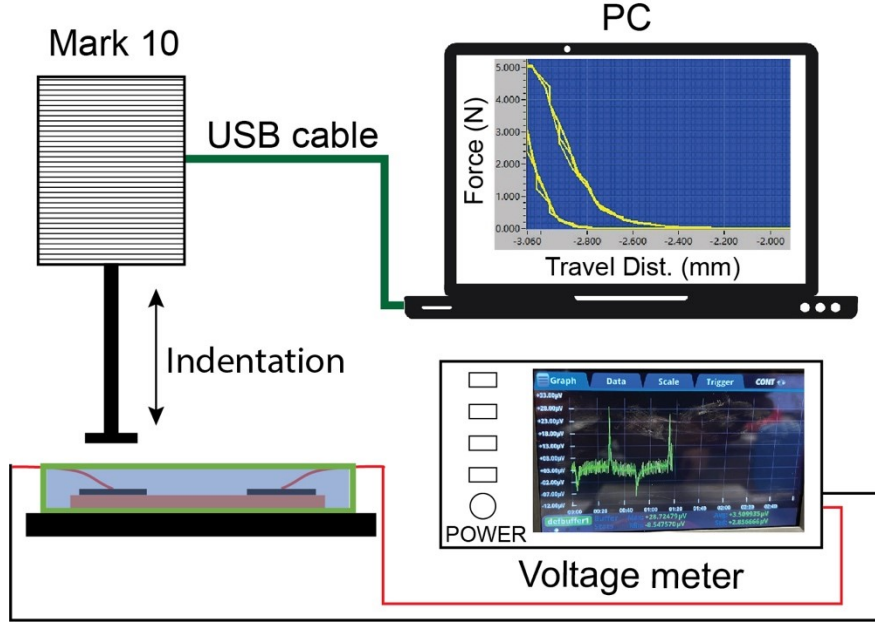
Figure S17. Schematical illustration of the home-made testing sytem for evaluating the mechano-electrical conversion of the piezoionic devices.
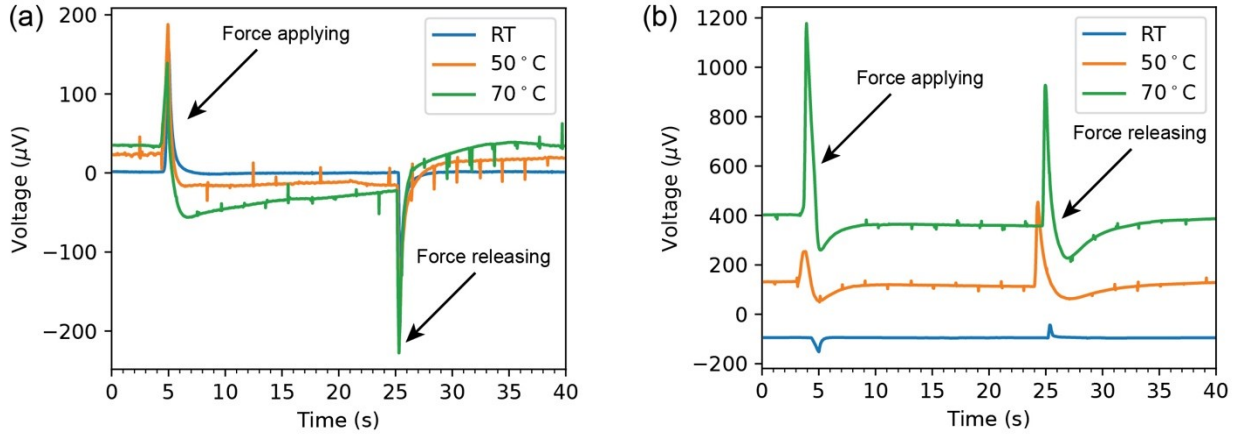
Figure S18. Generated voltage as a function of time in response to indentation for (a) P-type and (b) N-type piezoionic device at different temperatures.

For a piezoionic device, its generated voltage can be approximated as

$$V_1 \propto \frac{k}{D\mu}(\beta_+ - \beta_-)\nabla P \sim \frac{k}{D\mu}(\beta_+ - \beta_-)E \tag{S1}$$

For the full width at half maximum (FWHM) is related to the fluid flow speed and might be approximated as

$$\tau_1 \propto \frac{\mu}{k\nabla P} \sim \frac{\mu}{kE} \tag{S2}$$

The picture behind is that for hydrogel with a higher permeability k, the fluid flow is fast. Therefore, the generated voltage is higher and the FWHM is smaller. For a hydrogel with a lager Young's modulus E, for a give indentation depth, the pressure gradient ∇P is higher. Therefore, the fluid flow is faster, thus the generated voltage is higher and the FWHM is smaller. Similarly, for a hydrogel embedded with a less viscous fluid, i.e., a smaller μ, the fluid flow speed is faster according to the Darcy's law. Therefore, the generated voltage is higher and the FWHM is smaller. For ions with a lower diffusivity, ion diffusion, which counteracts the voltage generating streaming potential, is weaker. As a result, the generated voltage is higher. For the hindrance factor β, a higher mobility difference leads to a higher generated voltage.

The piezoionic effect depends critically on intrinsic material parameters k, E, μ, D, and β. Temperature affects all these intrinsic parameters. For example, a higher temperature leads to a higher ion diffusivity D and a lower viscosity of the fluid μ. The temperature might also affect the dissociation of the electrolytes in the hydrogel, thus changing the interaction between the ions and the polymer network, i.e., β. As the hydrogel consists of a polymer network with water imbedded inside and the stress of the polymer network can be described by a Flory-Huggins theory,

$$\sigma = \frac{Nk_bT}{\det F}(FF^T - I)$$

$$(S3)$$

where N is the number of polymer chains per unit volume, k_b is the Boltzmann constant, T is the temperature, F is the deformation gradient, and I is the second rank identity tensor. Evidently, the stress of the polymer depends on the temperature. As a result, its mechanical properties, i.e., E also depends on the temperature. In other words, the piezoionic effect depends critically on temperature through the temperature dependent intrinsic material parameters.

To quantify the dependence of piezoionic effect on temperature requires to quantify the relation between these intrinsic material parameters and the temperature first. Unfortunately, establishing such relation is not attainable at present.

Therefore, we have focused on operating parameters, i.e., indentation depth, indentation speed, electrode-stimulus center distance (spatial-temporal), that do not affect the intrinsic material parameters of the hydrogel in our manuscript. Importantly, the universal framework derived from our observations is independent on the intrinsic parameters, as long as the device operates through the piezoionic mechanism.

To demonstrate the complexity originates from the temperature effect, we have measured the voltage generation of P-type and N-type piezoionic devices in response to indentation when increasing the temperature, as shown in **Figure S18**.

During testing, the devices were heated on a heating stage to a prescribed temperature. The open circuit voltage (OCV) was recorded when the device was indented. There are some spikes on the curves at high temperature, which are due to electromagnetic interference (EMI) of the device by the heating stage. For the P-type piezoionic device, temperature does not affect the generated voltage significantly (**Figure S18a**). Nevertheless, temperature does modify the baseline of the device. However, for the N-type piezoionic device, temperature affects its voltage generation significantly. At room temperature, the N-type device operates normally. However, with

increasing temperature to 50˚C, an extra peak (with positive polarity) appears in advance of the normal response peak. Deviation from an ideal N-type piezoionic device is more evident when the temperature is increased to 70˚C. We suspect such deviation might be due to two aspects. First, we employ protonated chitosan to achieve the N-type piezoionic hydrogel. The protonation equilibrium might depend critically on the temperature. Therefore, when the temperature is increased to 70˚C, the protonation process changes dramatically, resulting in a change of the interaction between ions and the polymer chains, thereby leading to such deviation. Second, the temperature difference between the hydrogel and the indenter might result in instant heat transfer when the indenter is approaching the device, leading to a sudden temperature unbalance between the two electrodes of the device. Due to the temperature difference, an ionic thermoelectric effect[8] might occur, resulting in extra voltage generation process.
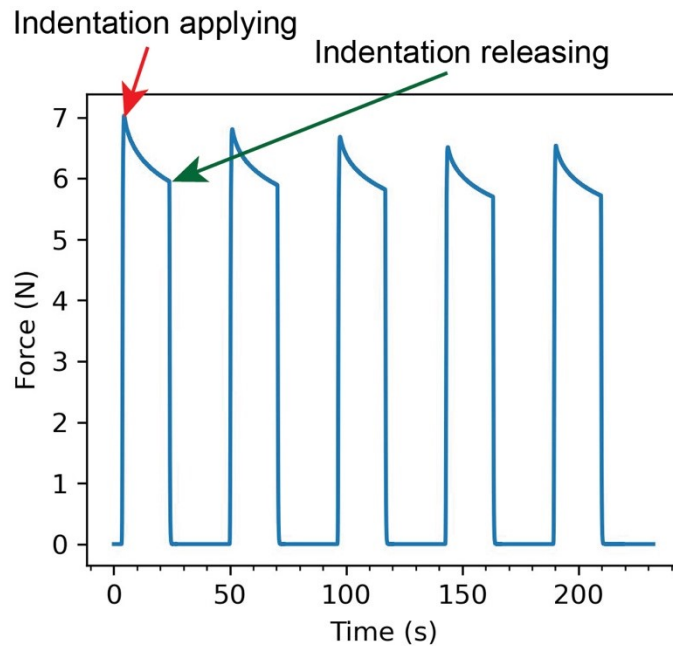
Figure S19. Measured force as a function of time during cyclic indentation test. It is noted that the force is also transient: during indentation, the force reaches it maximum then gradually decreases when even when the indentation is maintained.

The eqs. (1) – (9) were solved simultaneously using the MOOSE, which is an open source multiphysics framework based on C++. Details about how to solve a partial differential equation using MOOSE can be found on its website (https://mooseframework.inl.gov/). We briefly outline the steps for solving eqs. (1) – (8). First, the equations were transformed into their weak forms, including residual, Jacobian and off-diagonal Jacobian parts. Concepts of the weak form, residual, and Jacobians could be found on the MOOSE website or in a finite element method textbook.[9] Then the residual and Jacobians were translated into C++ codes by using the built-in test functions and shape functions in MOOSE according to its syntax. Finally, by defining the simulation domain, meshing the domain, and adopting proper boundary conditions, the equations were solved in MOOSE. It is noted during developing the C++ codes, Porous Flow and Tensor Mechanics Modules in MOOSE were used to account for the poroelasticity of the hydrogel.[10-12] **Figure S19** shows an example of force relaxation during indentation according to poroelasticity. One notable

difference from previous simulation is that the fluid in this study is modeled as compressible, which leads to more accurate results.

The device configurations adopted in simulation, including the device dimensions, electrode configurations, and indentation depths and speeds, are the same as the experimental ones, as shown in **Figure S14**. The boundary conditions were taken as follows:

i. For the electrical potential ψ, in case of spatial-temporal study, $\psi = 0$ on electrode 4; in case of dynamics study, $\psi = 0$ on the right electrode.

ii. For the cations and cation species as well as the solvent (water), zero flux boundary condition was adopted.

iii. For displacement, the bottom of the hydrogel were fixed because the hydrogel was constrained by the polyimide substrate. To simulate the indenting process, the y displacement of the hydrogel surface on top of the indented electrode was set to move downwards with the same speed as that in experiment during indentation. After reaching the prescribed indentation depth, the y displacement was maintained under its indented state. Similar displacement boundary condition was adopted during the indentation releasing process. Such constrain is important, as it is able to prevent relative motion between the electrode and the hydrogel, which might otherwise introduce suspicious voltage generation due to, e.g., triboelectric effect or electrical double layer charging.[4]

Discussion on the parameters used in the simulation

From eq.(S1), evidently, scaling k and D by the same factor does not change the generated voltage. The same is true for scaling E and D simultaneously. The same is also true for increasing k but decreasing E or decreasing k but increasing E by a same factor. In other words, there are degrees of freedom in choosing the material properties to fit the experiment results. To reduce the degree of freedoms requires techniques to measure five out of six parameters (k, D, E, β, ϕ and v) independently and accurately, which is challenging at present.
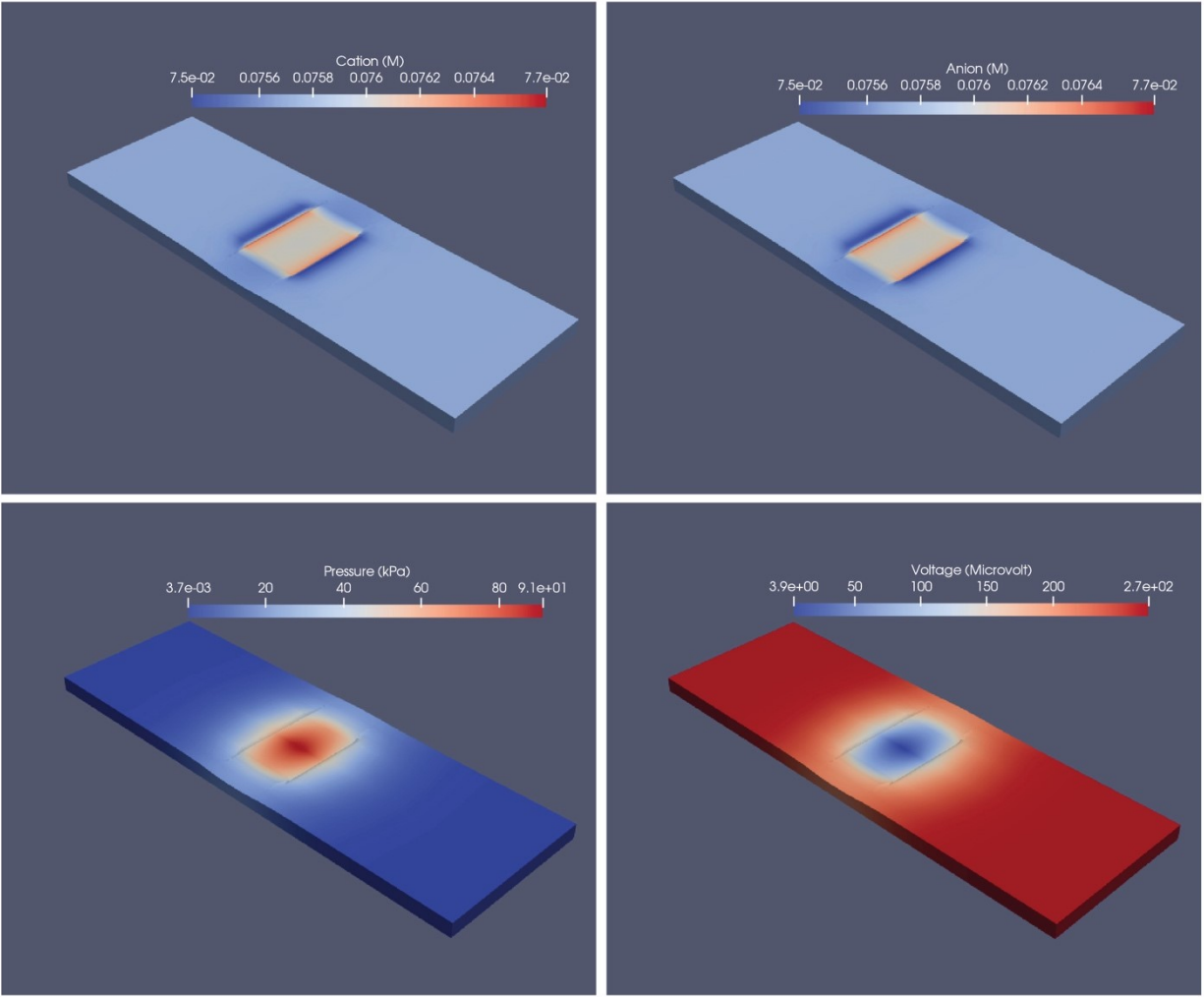
Figure S20. Snapshots of cation and anion concentrations, pressure, and voltage distributions corresponding the simulation results in **Figure 5a**. It is noted the snapshots are taken at the moment when the generated voltage is maximum.

Example of the cation and anion concentrations, pressure, and voltage distributions in simulation is presented in **Figure S20**. Snapshots were exported using ParaView.[13] Indentation induced pressure gradient generation thus voltage generation are evident.

Table S1. Parameters used in simulation for matching the transient behavior in **Figure 2** and the effect of stimulus strength on the piezoionic response in **Figure 3**.

Symbol	Model Parameter	Value (P-type)	Value (N-type)
E	Drained Young's modulus	220 kPa	213 kPa
ν	Poisson's ratio	0.499	0.499
k	Hydrogel permeability	5.2×10^{-15} m^2	5.3×10^{-15} m^2
ρ	Fluid density	1030 kg/m^3	1030 kg/m^3
G	Fluid bulk modulus	2.0 GPa	2.0 GPa
μ	Fluid viscosity	10 mPa·s	10 mPa·s
D_+	Cation diffusivity	2.4353×10^{-9} m^2/s	2.55×10^{-9} m^2/s
D_-	Anion diffusivity	2.4353×10^{-9} m^2/s	2.55×10^{-9} m^2/s
β_+	Cation hindrance factor	0.1	0.1
β_-	Anion hindrance factor	0.099	0.0995
T	Temperature	293.0 K	293.0 K
ϕ	Porosity	0.85	0.85

Note: The mass fractions of the ions species were estimated according to the recipes used in hydrogel synthesis. For the P-type piezoionic hydrogel, $\chi^+ = 1.69 \times 10^{-3}$ and $\chi^- = 1.29 \times 10^{-2}$. For the N-type piezoionic hydrogel, $\chi^+ = 1.22 \times 10^{-2}$ and $\chi^- = 2.61 \times 10^{-3}$. A more discussion on parameter choosing in the multiphysics modeling can be found in **Figure S18-S19**.

Table S2. Parameters used in simulation for matching the effect of stimulus speed on the piezoionic response in **Figure 4**.

Symbol	Model Parameter	Value (P-type)	Value (N-type)
E	Drained Young's modulus	220 kPa	213 kPa
ν	Poisson's ratio	0.499	0.499
k	Hydrogel permeability	5.2×10^{-15} m^2	5.3×10^{-15} m^2
ρ	Fluid density	1030 kg/m^3	1030 kg/m^3
G	Fluid bulk modulus	2.0 GPa	2.0 GPa
μ	Fluid viscosity	10 mPa·s	10 mPa·s
D_+	Cation diffusivity	2.852×10^{-9} m^2/s	2.55×10^{-9} m^2/s
D_-	Anion diffusivity	2.852×10^{-9} m^2/s	2.55×10^{-9} m^2/s
β_+	Cation hindrance factor	0.1	0.1
β_-	Anion hindrance factor	0.099	0.0995
T	Temperature	293.0 K	293.0 K
ϕ	Porosity	0.85	0.85

Table S3. Parameters used in simulation for matching the spatial-temporal distribution of the piezoionic response in **Figure 5** and **Figure 6**.

Symbol	Model Parameter	Value(P-type)	Value (N-type)
E	Drained Young's modulus	220 kPa	155 kPa
ν	Poisson's ratio	0.499	0.499
k	Hydrogel permeability	1.1×10^{-14} m^2	2.5×10^{-14} m^2
ρ	Fluid density	1030 kg/m^3	1030 kg/m^3
G	Fluid bulk modulus	2.0 GPa	2.0 GPa
μ	Fluid viscosity	10 mPa·s	10 mPa·s
D_+	Cation diffusivity	4×10^{-9} m^2/s	9×10^{-9} m^2/s
D_-	Anion diffusivity	4×10^{-9} m^2/s	9×10^{-9} m^2/s
β_+	Cation hindrance factor	0.1	0.1
β_-	Anion hindrance factor	0.09928	0.099625
T	Temperature	293.0 K	293.0 K
ϕ	Porosity	0.85	0.85

References

1.   Fievet, P.; Sbaï, M.; Szymczyk, A., Analysis of the Pressure-Induced Potential Arising across Selective Multilayer Membranes. *J. Membr. Sci.* **2005,** *264*, 1-12.

2.   Spiegler, K. S., On the Measurement of Streaming Potentials with Silver-Silver Chloride Electrodes. *Desalination* **1974,** *15*, 135-140.

3.   Prudnikova, K.; Utz, M., Electromechanical Equilibrium Properties of Poly(Acrylic Acid/Acrylamide) Hydrogels. *Macromolecules* **2012,** *45*, 1041-1045.

4.   Dobashi, Y.; Yao, D.; Petel, Y.; Nguyen, T. N.; Sarwar, M. S.; Thabet, Y.; Ng, C. L. W.; Scabeni Glitz, E.; Nguyen, G. T. M.; Plesse, C.; Vidal, F.; Michal, C. A.; Madden, J. D. W., Piezoionic Mechanoreceptors: Force-Induced Current Generation in Hydrogels. *Science* **2022,** *376*, 502-507.

5.   Wu, J., Understanding the Electric Double-Layer Structure, Capacitance, and Charging Dynamics. *Chem. Rev.* **2022,** *122*, 10821-10859.

6.   Zou, H.; Zhang, Y.; Guo, L.; Wang, P.; He, X.; Dai, G.; Zheng, H.; Chen, C.; Wang, A. C.; Xu, C.; Wang, Z. L., Quantifying the Triboelectric Series. *Nature Communications* **2019,** *10*, 1427.

7.   Zhang, R.; Olin, H., Material Choices for Triboelectric Nanogenerators: A Critical Review. *EcoMat* **2020,** *2*, e12062.

8.   Han, C.-G.; Qian, X.; Li, Q.; Deng, B.; Zhu, Y.; Han, Z.; Zhang, W.; Wang, W.; Feng, S.-P.; Chen, G.; Liu, W., Giant Thermopower of Ionic Gelatin near Room Temperature. *Science* **2020,** *368*, 1091-1098.

9.   Langtangen, H. P.; Mardal, K.-A., *Introduction to Numerical Methods for Variational Problems*. Springer Nature: **2019;** Vol. 21.

10.   Adhikary, D. P.; Jayasundara, C. T.; Podgorney, R. K.; Wilkins, A. H., A Robust Return-Map Algorithm for General Multisurface Plasticity. *International Journal for Numerical Methods in Engineering* **2017,** *109*, 218-234.

11.   Wilkins, A.; Green, C. P.; Ennis-King, J., Porousflow: A Multiphysics Simulation Code for Coupled Problems in Porous Media. *Journal of Open Source Software* **2020,** *5*, 2176.

12.   Cheng, A. H.-D., *Poroelasticity*. Springer: **2016;** Vol. 27.

13.   Ayachit, U., *The Paraview Guide: A Parallel Visualization Application*. Kitware, Inc.: **2015**.